Functional Analysis of Common and Rare Cystic Fibrosis-causing Mutations

PhD thesis

Olivér Závoti

Semmelweis University Doctoral College
Molecular Medicine Division

Supervisor:	László Csanády, MD, DSc
Official reviewers:	Gábor Czirják, MD, DSc Gábor Tibor Szántó, PhD
Complex Examination:	
Head:	Péter Várnai, MD, DSc
Members:	László Homolya, DSc Gergely Szakács, MD, PhD

Budapest
2026

1. Introduction

The Cystic Fibrosis Transmembrane Conductance Regulator (CFTR) is an ATP-regulated anion channel, primarily transporting chloride (Cl^-) and bicarbonate (HCO_3^-) ions across epithelial cell membranes. CFTR is highly expressed in the airways, pancreas, intestine, and sweat glands, where it regulates fluid secretion, mucus hydration, and electrolyte balance.

Structurally, CFTR consists of two transmembrane domains (TMDs), two nucleotide-binding domains (NBD1 and NBD2), and a unique regulatory (R) domain. Channel activation is controlled by binding and phosphorylation of the R domain by protein kinase A (PKA) and channel gating is fuelled by ATP binding/hydrolysis at the NBDs.

Mutations in the CFTR gene cause cystic fibrosis, one of the most common lethal inherited disorders in populations of European descent. More than 2,000 CFTR variants have been identified, although only a subset are disease-causing. The most prevalent mutation, ΔF508 (F508del), results in protein misfolding and defective trafficking, leading to degradation before the protein reaches the cell surface. Other mutations may impair channel gating, conductance, or stability. Dysfunctional CFTR causes dehydrated mucus, chronic lung infections, pancreatic insufficiency, and elevated sweat chloride levels.

Current therapies for cystic fibrosis have shifted from symptomatic treatment to mutation-targeted therapies. CFTR modulators include potentiators such as ivacaftor, which enhance channel opening, and correctors such as tezacaftor and elexacaftor, which improve protein folding and trafficking. Combination therapies, particularly elexacaftor/tezacaftor/ivacaftor (ETI), have significantly improved lung function and quality of life for many patients with CF.

2. Objectives

Cystic fibrosis-causing mutations impair CFTR channel function through diverse defects in protein biogenesis, regulation, and gating. The overall aim of this thesis is to define the molecular and functional consequences of common and rare pathogenic CFTR mutations and to evaluate their responsiveness to the ETI CFTR modulator combination.

Although the ΔF508 and G551D mutations have been extensively studied for their effects on ATP-dependent gating, both also display impaired PKA-dependent activation. Here, we aim to characterise the defects in PKA-dependent activation of ΔF508 and G551D CFTR and to determine how clinically used modulators influence channel activation and gating.

Recent studies identified several rare CF-causing missense mutations in the Hungarian CF population, including G126D, I336K, T465I, T582I, and D984V, whose functional and pharmacological properties remain poorly understood. We aim to characterise the effects of these mutations on CFTR biogenesis and channel function, and to evaluate their responsiveness to currently available CFTR potentiator and corrector therapies, thereby supporting the extension of precision-medicine approaches to rare CFTR variants.

3. Methods

3.1. Molecular biology and expression systems

CFTR mutations were introduced into human CFTR/pGEMHE and CFTR/pcDNA3 constructs by site-directed mutagenesis and verified by sequencing. For electrophysiological studies, cRNAs were synthesised *in vitro* and injected into *Xenopus laevis* oocytes. Recordings were performed 1-4 days after injection. For biochemical

experiments, HEK-293T cells were transiently transfected with CFTR constructs using Lipofectamine 3000.

3.2. Inside-out patch clamp recordings

CFTR channel activity was studied in excised inside-out membrane patches from *Xenopus laevis* oocytes using standard patch-clamp techniques. Macroscopic and single-channel currents were recorded at 25°C using an Axopatch 200B amplifier and digitised with a Digidata 1550B interface. Rapid solution exchange enabled controlled application of ATP, PKA, and CFTR modulators, including ivacaftor (VX-770) and elexacaftor (VX-445). Current recordings were analysed to determine channel open probability, burst duration, interburst duration, and opening/closing rates using dwell-time analysis and kinetic modeling.

3.3. Western blot analysis

To assess CFTR protein expression and maturation, crude membrane fractions were prepared from transfected HEK-293T cells. Proteins were separated by SDS-PAGE and transferred to nitrocellulose membranes. CFTR was detected using the 5E2 monoclonal antibody against the NBD2 domain, followed by alkaline-phosphatase-conjugated secondary antibodies and colorimetric detection. Band intensities corresponding to immature (Band B) and mature (Band C) CFTR were quantified by densitometric analysis by fitting Gaussian functions to the lane densitometric profiles.

3.4. Statistics

Data are presented as mean ± SD. Electrophysiological sample size (n) represents the number of excised patches. Statistical significance was determined using Student's t-test, with $p < 0.05$ considered significant.

4. Results

4.1. Interactions of the the ΔF508 and G551D mutants and the catalytic subunit of PKA

4.1.1. Increased noncatalytic activation by PKA for both ΔF508 and G551D CFTR in the presence of an ATP analogue

N^6-(2-phenylethyl)-ATP (P-ATP) is a high-affinity ATP analogue that is able to bind to the CFTR protein and drive channel gating; however, P-ATP cannot bind to PKA and thus cannot support phosphorylation. Consequently, noncatalytic (reversible) CFTR activation mediated by PKA binding can be selectively assessed by applying PKA to channels that are gating in the presence of P-ATP. Inside-out membrane patches from *Xenopus laevis* oocytes expressing ΔF508 or G551D CFTR mutants were sequentially exposed for approximately ~1-min intervals to 300 nM PKA under three conditions: in the presence of, first, P-ATP (10 μM), then ATP (2 mM), and finally P-ATP again (Fig. 1). The application of PKA in P-ATP selectively elicited noncatalytic stimulation of non-phosphorylated and phosphorylated channels, respectively. PKA application in ATP induced both catalytic (irreversible) activation, due to phosphorylation, and noncatalytic activation which manifested as a partial current decline after the removal of PKA (Fig. 1A and B, centre; Fig. 1C and D, second blue arrow). Notably, in our inside-out patch experimental setting, noncatalytic activation is rapidly reversible upon PKA washout, in contrast to catalytic activation, which is considered irreversible due to the absence of cytosolic phosphatases that dephosphorylate CFTR in intact cells.

For both variants, noncatalytic activation by PKA was detectable both prior and following phosphorylation. However, the reversible component of activation of the phosphorylated channels was substantially larger in P-ATP than in ATP (Fig. 1, compare second and third blue double arrows), by more than 2-fold for ΔF508 and by

approximately 10-fold for G551D CFTR. Moreover, for ΔF508 CFTR, noncatalytic stimulation of non-phosphorylated channels in P-ATP was approximately 2-fold larger than that observed for phosphorylated channels in ATP (Fig. 1, compare first and second blue double arrows). These findings contrast with wild-type CFTR, for which the amplitude of the noncatalytic current component is largely independent of whether ATP or P-ATP is used to drive channel gating (Fig. 1, blue double arrows; data replotted from Mihályi et al., 2020).

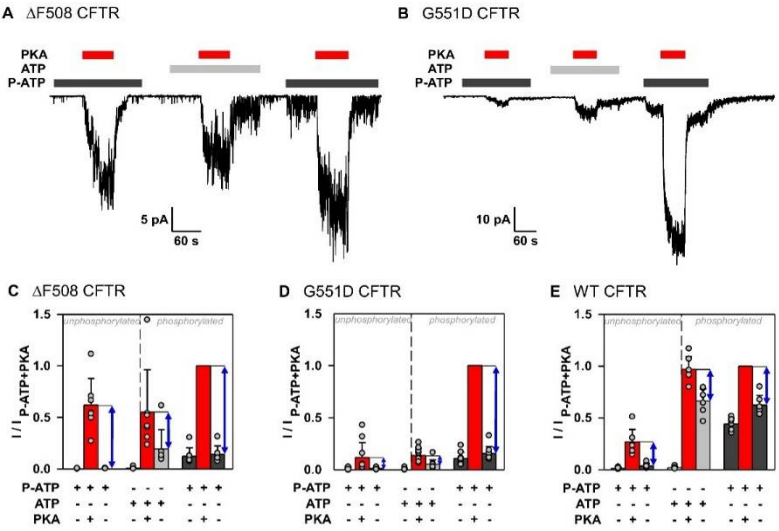

Figure 1. Noncatalytic activation of ΔF508 and G551D CFTR by PKA is enhanced in the presence of P-ATP.

4.1.2. Slower activation by PKA for both ΔF508 and G551D CFTR channels

Literature suggests slower activation by PKA of both ΔF508 and G551D CFTR, raising the possibility that the 1-min ATP + PKA exposure used in our protocol shown in Fig. 1A-B may not suffice to achieve complete phosphorylation. To address this, we examined

current activation for both mutants over prolonged PKA application (~4 minutes; Fig. 2A, D). Confirming previous findings, current activation of ΔF508 CFTR was markedly delayed as the current reached only ~50% of its maximal level after a 1-minute exposure to ATP + PKA (Fig. 2A) in comparison with WT CFTR, for which ~90% of the maximal current develops within one minute. As for G551D CFTR, the extended exposure in ATP + PKA (Fig. 2D) did not indicate reduced fractional activation after the first minute. Of note, the small amplitudes and pronounced stochastic fluctuations of G551D currents limit the reliability of this approach.

To estimate the activation half-times of the mutant channels, we constructed macroscopic currents for both mutants by summing currents from eight patches aligned to the onset of PKA application (Fig 2 B, E). Analysis of these summed currents yielded activation half-times ($t_{1/2}$) of ~40 s for ΔF508 and ~29 s for G551D CFTR (Fig. 2 B and E; L-bars and black numbers), both of which were substantially prolonged compared to WT CFTR ($t_{1/2}$ = 11.8 ± 1.4 s, n = 13; Fig. 2B and E, blue traces).

Notably, the ratio between reversible (noncatalytic) and irreversible (catalytic) components of activation was also altered in both mutants. For WT CFTR channels exposed to 300 nM PKA, these components contribute approximately equally to the total current. On the other hand, for phosphorylated ΔF508 and G551D CFTR, the total current measured in ATP + PKA was dominated by the reversible component. Macroscopic currents generated by summing patch currents synchronised to PKA washout (Fig. 2C and F) indicate that, in both mutants, the reversible component accounts for ~75-80% of the total current, whereas the irreversible component contributes only ~20-25%. Therefore, both mutations impair catalytic activation to a greater extent than noncatalytic activation.

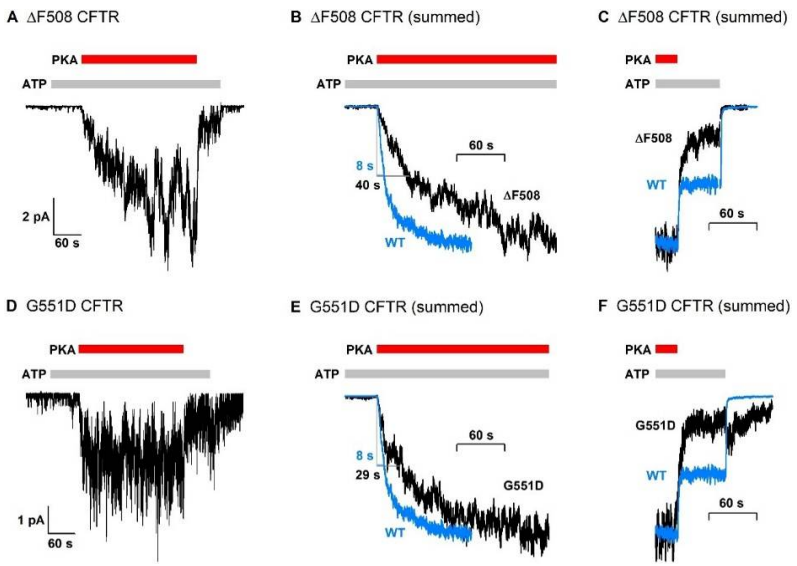

Figure 2. PKA-evoked ΔF508 and G551D CFTR currents develop slower than WT and are dominated by noncatalytic activation.

Although the data in Fig. 2B suggests that ΔF508 channels did not reach full phosphorylation under the protocol used in Fig. 1A, the marked enhancement of noncatalytic stimulation in the presence of P-ATP was confirmed using longer PKA exposures (>2 min in P-ATP and ~4 min in ATP). Because prolonged recordings led to substantial current rundown in some patches, currents measured during the three consecutive segments (P-ATP, ATP, P-ATP) were analysed separately and normalised to the current recorded in the presence of PKA within each respective segment. These experiments again demonstrated a strong enhancement of noncatalytic stimulation of phosphorylated ΔF508 channels by PKA in P-ATP compared with ATP (Fig. 2A, C), as reflected by the larger fractional stimulation. Consistent with the dominance of noncatalytic activation in total ΔF508 channel activity in ATP + PKA (Fig. 2A), removal of PKA produced a larger fractional current decrease than observed for WT channels.

4.1.3. In the presence of potentiators, the reversible component of activation is undetectable for phosphorylated ΔF508, but is retained for G551D CFTR

Because most CF patients carrying ΔF508 alleles are currently treated with the ETI triple-combination therapy, we examined how the two potentiator components, elexacaftor and ivacaftor, together modulate PKA-dependent activation of ΔF508 CFTR. Unphosphorylated ΔF508 channels produced robust macroscopic currents in the presence of 10 μM P-ATP, 1 μM elexacaftor and 10 nM ivacaftor, indicating notable drug-induced channel activation even prior to phosphorylation (Fig. 3A, left; cf. Fig. 1A, left). Exposing the channels to 300 nM PKA for 1 minute strongly enhanced these currents, demonstrating pronounced noncatalytic activation of unphosphorylated ΔF508 CFTR even in the presence of the potentiators (Fig. 3A-B).

Then, we examined PKA-dependent activation in the presence of ATP together with elexacaftor and ivacaftor (Fig. 3C-D). Once again, the exposure of unphosphorylated ΔF508 CFTR channels to ATP plus the drugs generated macroscopic currents, which increased by only ~2-3-fold during a 4-minute exposure to 300 nM PKA (Fig. 3C; Fig. 3D, 2nd vs. 1st bar), in contrast to the ~80-fold stimulation observed in the absence of drugs (Fig. 1A, centre). Unexpectedly, removal of PKA in the continued presence of the drugs did not result in a significant current decrease, indicating a near-complete lack of noncatalytic stimulation of phosphorylated ΔF508 CFTR channels under these conditions (Fig. 3C, right; Fig. 3D, 3rd vs. 2nd bar). Interestingly, noncatalytic stimulation of phosphorylated ΔF508 CFTR in the presence of ivacaftor alone has been demonstrated previously (Fig. 3E, replotted from Mihályi et al., 2024). In this study, we therefore also assessed PKA-dependent activation in the presence of elexacaftor alone (Fig. 3F-G). Under this condition, PKA dependence of ΔF508 CFTR activity closely resembled that reported

for ivacaftor alone. Exposure of unphosphorylated ΔF508 channels to elexacaftor and ATP failed to elicit macroscopic currents (Fig. 3F, left; Fig. 3G, 1st bar). Following full channel activation, PKA removal triggered a rapid and pronounced current decline (Fig. 3F, right; Fig. 3G, 3rd vs. 2nd bar). Taken together, these results demonstrate that noncatalytic stimulation of phosphorylated ΔF508 CFTR by PKA is preserved in the presence of either ivacaftor or elexacaftor alone but is abolished when both potentiators are applied simultaneously.

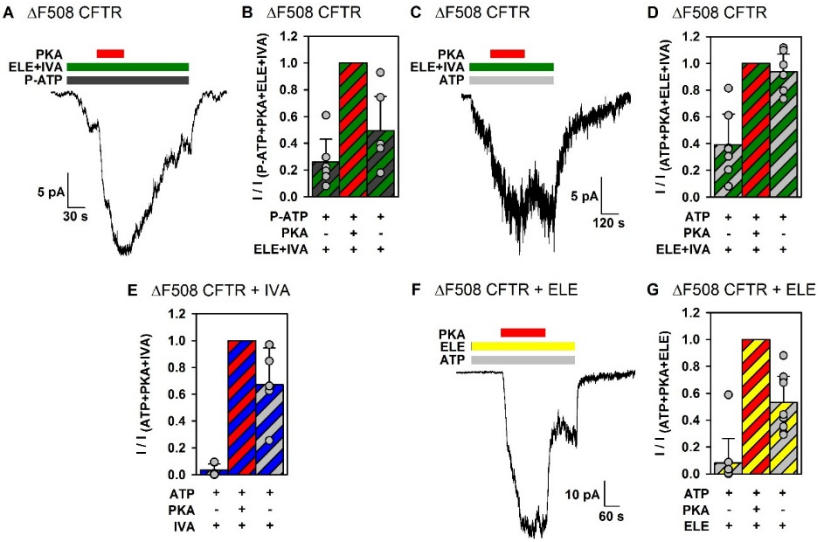

Figure 3. Effects of potentiator drugs ΔF508 CFTR.

The absence of noncatalytic stimulation of ΔF508 CFTR by PKA in the presence of ATP + ivacaftor + elexacaftor was further confirmed in recordings from patches containing only a small number of active channels, enabling dwell-time analysis. The estimated open probability of phosphorylated channels in ATP + drugs remained ~0.5 and was unaffected by the presence or absence of PKA.

Although most patients carrying a G551D allele can be treated with ivacaftor monotherapy, many, particularly those who also carry a ΔF508 allele, have transitioned to ETI therapy. In intact cells, combined treatment with elexacaftor and ivacaftor has been reported to increase forskolin-stimulated G551D CFTR activity by approximately two orders of magnitude. We also examined how elexacaftor and ivacaftor modulate catalytic and noncatalytic PKA-dependent activation of G551D CFTR. PKA, applied to unphosphorylated channels gating in P-ATP in the presence of elexacaftor and ivacaftor, produced a pronounced reversible stimulation. Moreover, currents from unphosphorylated G551D channels gating in ATP together with the two drugs were robustly enhanced by PKA, indicating that the open probability of unphosphorylated G551D CFTR remains low even in the presence of both potentiators. This behaviour contrasts with that observed for ΔF508 CFTR (Fig. 3C, left; Fig. 3D, 1st vs. 2nd bar). Finally, removal of PKA revealed that about ~50% of the total current observed in the presence of ATP + PKA + drugs arose from reversible, noncatalytic stimulation. Altogether, the elexacaftor-ivacaftor combination preserves and boosts both catalytic and noncatalytic components of activation of G551D CFTR channels.

4.2. Characterisation of rare, cystic fibrosis-causing mutations

4.2.1. Channel maturation of the five mutants is variously compromised and can be restored by the correctors

Normally, CFTR undergoes sequential glycosylation, beginning with core glycosylation in the ER and followed by complex glycosylation in the Golgi apparatus. As glycosylation decreases electrophoretic mobility, the different maturation states of CFTR can be separated by SDS-PAGE. Western blot analysis of wild-type (WT) CFTR typically reveals three distinct bands (Fig. 4A, left), corresponding to

the non-glycosylated (Band A), core-glycosylated (Band B), and fully mature, complex-glycosylated (Band C) forms. Class II CFTR mutations, including ΔF508, disrupt proper protein folding and maturation, resulting in ER retention and a marked reduction or absence of Band C.

To evaluate the impact of the five rare CFTR mutations on protein expression and maturation, we compared their electrophoretic migration profiles by western blot analysis of crude membrane preparations from HEK-293T cells transiently expressing each mutant construct (Fig. 4A). Densitometric quantification demonstrated a reduction in Band C intensity for all five variants relative to WT CFTR, with the most pronounced decreases observed for I336K and T465I, which reached approximately 38% and 14% of WT levels, respectively. In contrast, the intensities of Bands A and B were not reduced for any mutant. Consequently, the fractional contribution of Band C to total CFTR signal [C/(A + B + C)] was significantly diminished for I336K ($p = 0.0116$), T465I ($p = 4.99 \times 10^{-5}$), and T582I ($p = 0.0493$). Given that Band C abundance correlates with CFTR surface expression, these findings indicate reduced plasma membrane localisation of all mutant channels, with I336K and T465I exhibiting the most severe defects, classifying them as Class II (folding and trafficking) mutants.

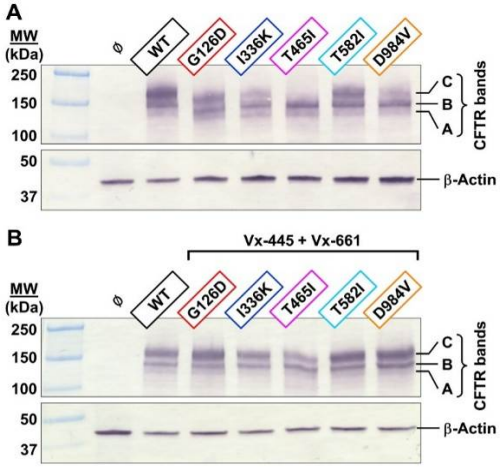

Figure 4. Impaired maturation of mutant CFTR channels and rescue by corrector treatment.

The correctors tezacaftor and elexacaftor have been shown to effectively rescue the maturation of Class II CFTR mutants, including ΔF508, as well as numerous rare variants. To determine the responsiveness of the five CFTR mutants examined here, cells were treated for 24 hours with 3 μM tezacaftor and 3 μM elexacaftor before protein extraction; these drug concentrations are reportedly physiologically relevant and have been proven efficient for multiple CFTR variants in vitro. Corrector treatment increased Band C intensity for all five mutants (Fig. 4A vs. Fig. 4B), and the magnitude of rescue inversely correlated with the baseline Band C levels observed under untreated conditions; the strongest responses were observed for T465I and I336K. All in all, the correctors restored Band C levels to near WT values for all mutants.

4.2.2. While ATP affinity and activation by PKA remain intact, single-channel recordings reveal gating defects for G126D, T582I and D984V CFTR

WT CFTR and all five variants were expressed in *Xenopus laevis* oocytes and analysed using inside-out patch clamp recordings. Application of 2 mM ATP + 300 nM PKA activated large macroscopic currents for the G126D, T582I, and D984V mutants. In contrast, only sporadic pore openings were observed for I336K and T465I under identical conditions, even after injection of up to 30 ng of cRNA. Accordingly, gating properties could be quantitatively characterised only for G126D, T582I, and D984V CFTR.

All three mutants exhibited wild-type-like regulation by PKA, with negligible activity in ATP prior to PKA exposure, robust activation upon PKA application, and rapid partial deactivation following PKA washout. Notably, the fraction of current persisting after PKA removal was slightly but significantly reduced for all three mutants compared to WT ($p = 0.000597$, 0.00009, and 0.0223 for G126D, T582I, and D984V, respectively), suggesting a modest increase in the relative contribution of the reversible component to total channel activity in the mutants.

The ATP sensitivity of pre-phosphorylated channels was assessed by exposing patches containing multiple channels to various test ATP concentrations bracketed by applications of 3.2 mM ATP. All three mutants displayed intact ATP sensitivity, yielding dose-response curves indistinguishable from WT ($K_{1/2} \approx 50$ μM).

To compare steady-state gating kinetics of the mutant channels to the wild type, currents of pre-phosphorylated WT, G126D, T582I, and D984V CFTR were recorded in the presence of 2 mM ATP from patches containing only a few channels ($N \leq 5$), allowing individual gating events to be clearly resolved (Fig. 5A, left). To estimate channel number within each patch, 300 nM PKA was reapplied at the

end of each recording to elicit noncatalytic stimulation and ATP was replaced by 50 μM 2-deoxy-N^6-(2-phenylethyl)adenosine-5-O-triphosphate (P-dATP), a nucleotide analogue that directly stimulates CFTR gating by binding to its nucleotide-binding domains. This protocol produces strong activation of CFTR channels (Fig. 5A, right). Open probability (P_o), mean burst duration (T_b), and mean interburst duration (T_{ib}) were quantified by dwell-time analysis.

Compared to WT CFTR, Po was only modestly reduced for D984V, but was significantly decreased for G126D ($p = 0.00194$) and T582I ($p = 0.000195$) (Fig. 5B, right), classifying the latter two variants as Class III (gating) mutants. The kinetic mechanisms underlying the reduced Po differed among mutants: for G126D, the P_o reduction resulted primarily from an increased closing rate, reflected by a shortened T_b ($p = 0.00266$), whereas for T582I it was caused by a decreased opening rate, manifested as a prolonged T_{ib} ($p = 0.000865$). In contrast, D984V exhibited an increased closing rate that was partially compensated by a concomitant increase in opening rate (Fig. 5B, bottom).

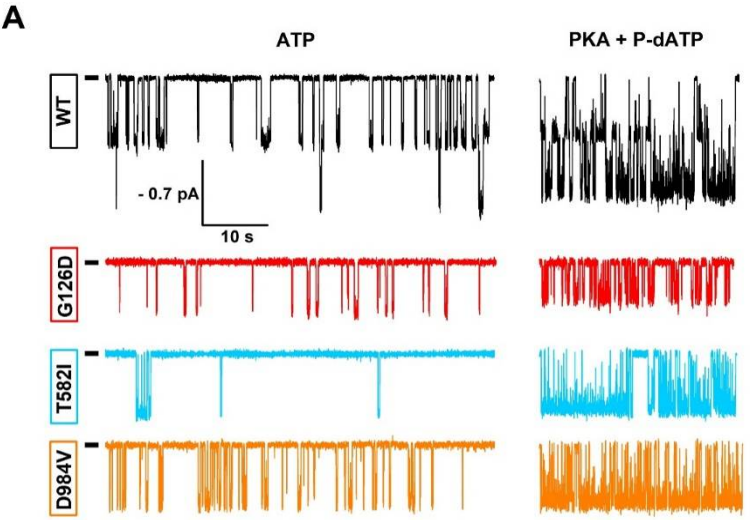

B

Construct	n	Parameter		
		Opening rate (s^{-1})	Closing rate (s^{-1})	P_o
WT	11	0.45 ± 0.24	2.56 ± 1.53	0.16 ± 0.06
G126D	11	0.46 ± 0.36	5.11 ± 1.93	0.08 ± 0.05
T582I	7	0.07 ± 0.03	1.41 ± 0.54	0.04 ± 0.03
D984V	10	0.62 ± 0.37	4.22 ± 1.24	0.12 ± 0.07

Figure 5. Single-channel recordings reveal reduced open probability of G126D and T582I CFTR.

4.2.3. Potentiators enhance gating of all five variants including I336K and T465I

We employed macroscopic inside-out patch-clamp recordings to determine the extent to which the gating defects of the G126D, T582I, and D984V CFTR variants can be rescued by potentiator drugs. In addition to the potentiator ivacaftor, the corrector elexacaftor has been shown to function as a co-potentiator that synergistically enhances CFTR gating. Pre-phosphorylated channels gating in the presence of 2 mM ATP were first exposed to 10 nM ivacaftor (Fig. 6A-C), a clinically relevant free drug concentration that is near-saturating for WT CFTR and many mutant channels.

After current stabilisation, 1 μM elexacaftor was added (Fig. 6A-C), a concentration well above the reported EC_{50} values for co-potentiation (1-15 nM) across WT CFTR and multiple variants. To achieve maximal stimulation, 300 nM PKA was subsequently reapplied, and ATP was replaced by 50 μM P-dATP, while maintaining both potentiators throughout (Fig. 6A-C). All three mutants responded robustly to the drugs combination (Fig. 6F; note logarithmic scale). Ivacaftor alone increased macroscopic currents by ~ 3-5-fold (Fig. 6F, 1st panel), while the addition of elexacaftor produced a further ~2-fold potentiation (Fig. 6F, 2nd panel). Consequently, the combined drug treatment enhanced currents by ~4-fold for D984V, ~6-fold for G126D, and ~10-fold for T582I. Despite this substantial rescue, the open probability (P_o) of all three mutants remained well below unity, as indicated by the additional current increases observed upon the application of PKA and subsequent substitution of ATP with P-dATP (Fig. 6F, 3rd and 4th panels).

Of note, the maximal stimulation achieved with the full stimulator cocktail provides an upper bound for the initial P_o in the presence of ATP alone. For T582I and D984V, these upper bounds are consistent with P_o values obtained from single-channel recordings (Fig. 5B). In contrast, for G126D the approximately 20-fold maximal stimulation (Fig. 6F, 4th panel, red symbol) implies an initial P_o of $\leq$~0.05, suggesting a slight overestimation of P_o in the single-channel analysis (Fig. 5), most likely due to uncertainties in determining channel number in the patch.

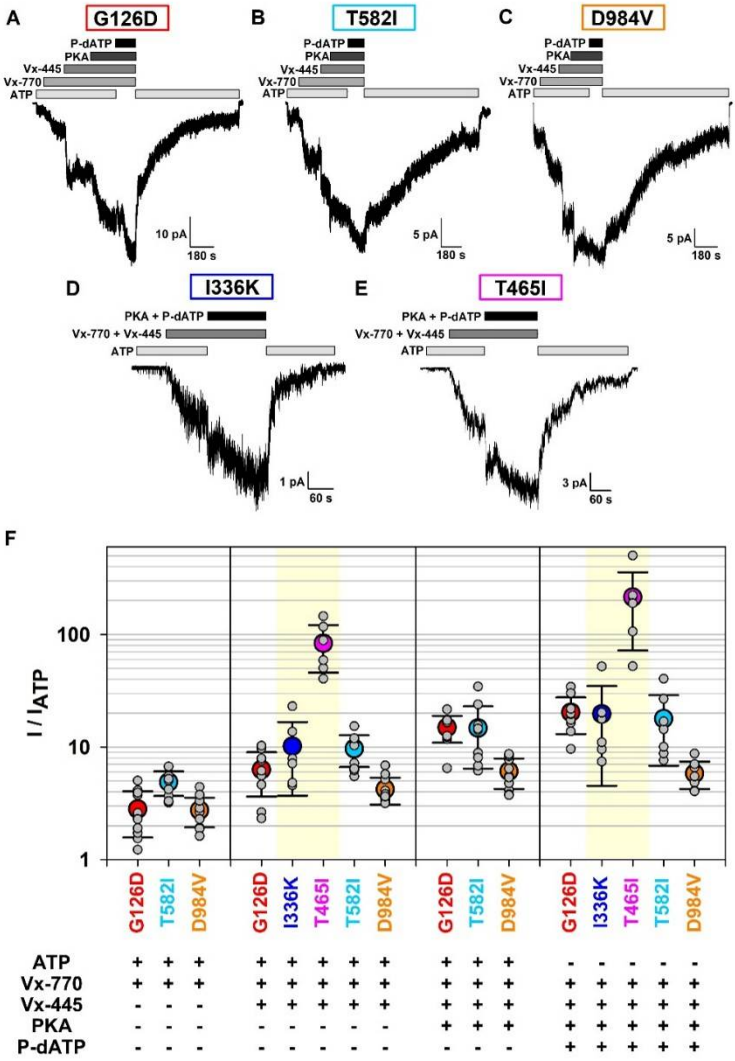

Figure 6. All mutant CFTR channels respond to potentiator treatment.

For the I336K and T465I variants, the lack of macroscopic currents with PKA and ATP alone may only be partially attributed to their maturation defects (Fig. 4). We therefore tested whether these mutants also exhibit intrinsic gating defects and whether they respond to potentiator drugs. Indeed, exposure of pre-phosphorylated channels to 10 nM ivacaftor + 1 μM elexacaftor activated large macroscopic currents in both cases (Fig. 6D-E), corresponding to approximately 10-fold and 80-fold current increases for I336K and T465I, respectively (Fig. 6F, 2nd panel). Subsequent addition of PKA and P-dATP further enhanced these currents by roughly two-fold (Fig. 6D-E), yielding maximal fractional stimulations of ~20-fold for I336K and ~200-fold for T465I CFTR. These results imply that, in the presence of ATP alone, P_o is $\leq$~0.05 for phosphorylated I336K and $\leq$~0.005 for phosphorylated T465I, classifying both variants as Class III (gating) mutants as well.

Although even rough estimates of channel number in a patch are not feasible for the latter two mutants, dwell-time analysis of record segments obtained in ATP alone, prior to drug application (Fig. 6D-E, initial segments), permits accurate estimation of the closing rate. Together with the upper bounds for P_o described above, this information allows calculation of an upper bound for the opening rate. This detailed kinetic analysis again revealed distinct mechanisms underlying impaired gating in the two mutants. The closing rate was only modestly increased (T_b shortened) for T465I but markedly accelerated for I336K, whereas the opening rate was dramatically reduced (T_{ib} prolonged; >20-fold) for T465I but likely less affected for I336K.

4.2.4. Small reductions in unitary current amplitude for G126D, I336K, and T465I

Single-channel current amplitudes for T582I and D984V CFTR were similar to that of WT (Fig. 5A), whereas visibly smaller amplitudes were observed for the remaining three mutants. To quantify these

differences, unitary conductances were determined by measuring single-channel current amplitudes at membrane potentials of -80, -40, and +40 mV. Linear regression of the resulting current-voltage relationships yielded slope conductances for each variant. Relative to WT CFTR (7.3 ± 0.6 pS), unitary conductance was modestly but significantly reduced for G126D (6.1 ± 0.1 pS; p = 0.00270), I336K (5.0 ± 0.3 pS; p = 0.00001), and T465I (6.4 ± 0.5 pS; p = 0.00975), classifying these three variants also as Class IV mutants.

5. Conclusions

5.1. Interactions of the ΔF508 and G551D mutants and the catalytic subunit of PKA

- Foth ΔF508 and G551D CFTR, non-catalytic activation dominates overall channel activity and may be further enhanced by stabilisation of the NBD1-NBD2-TMD interface via P-ATP.
- Both ΔF508 and G551D mutants exhibit slowed PKA-dependent activation, despite retaining normal binding affinity for the kinase.
- For ΔF508 CFTR, clinically used potentiators induce substantial PKA-independent activity, but also suppress non-catalytic activation of phosphorylated channels.

5.2. Characterisation of rare, cystic fibrosis-causing mutations

- Channel glycosylation is mildly impaired for G126D and T582I, substantially reduced for I336K and D984V, and severely disrupted for T465I. Treatment with clinically approved corrector compounds restores glycosylation to near wild-type levels.

- Channel open probability is mildly reduced for D984V, substantially decreased for G126D, and severely impaired for I336K, T465I, and T582I. Potentiator treatment markedly improves channel gating, resulting in substantial increases in macroscopic currents across all five variants.
- Channel conductance is mildly decreased for mutations G126D, I336K, and T465I.
- Collectively, these *in vitro* findings suggest that ETI therapy is likely to provide clinical benefit for patients carrying any of these five mutations.

6. Bibliography of the candidate's publications

Publications related to the thesis:

– Závoti O, Simon MA, Csanády L. Altered functional interactions between CFTR disease mutants DeltaF508 and G551D and the protein kinase A catalytic subunit. *J Physiol*. 2026; 604(8):3344-3362. doi: 10.1113/JP290798.

– Závoti O, Csanády L. Molecular and pharmacological evaluation of rare, cystic fibrosis-causing missense mutations of the CFTR channel. *J Physiol*. 2025;603(19):5437-5453. doi:10.1113/JP288955

Publications not related to the thesis:

– Voniatis C, Závoti O, Manikion K, Budavári B, Hajdu AJ. Fabrication of Mechanically Enhanced, Suturable, Fibrous Hydrogel Membranes. Membranes (Basel). 2023;13(1):116. Published 2023 Jan 16. doi:10.3390/membranes13010116

∑IF: 12,1